Thermodynamics of a correlated confined plasma II. Mesoscopic system

Institute of Physics Publishing Journal of Physics: Conference Series **35** (2006) 94–109
doi:10.1088/1742-6596/35/1/008 Progress in Nonequilibrium Green's Functions III

Thermodynamics of a Correlated Confined Plasma II. Mesoscopic System

Wolf Dietrich Kraeft[1,2] **and Michael Bonitz**[2]

[1] Institut für Physik, Universiät Greifswald, Domstr. 10a, D-17489 Greifswald
[2] Institut für Theoretische Physik und Astrophysik, Universität Kiel, Leibnizstr.15, D-24098 Kiel

E-mail: wolf-dietrich.kraeft@uni-rostock.de

Abstract. Finite systems of charge carriers confined by a harmonic trap are considered. The onion shell model for Coulomb clusters is analyzed and an improved model is proposed which is able to more accurately reproduce the results of numerical experiments. The ground state energy is determined, and the transition to an infinite system is discussed.

1. Introduction

The investigation of particles in a trap is of high current interest in many fields. Examples are bose condensates of alkali metals, electrons in quantum confined semiconductor structures, e.g. [1, 2], ions in Penning and Paul traps, e.g. [3] and dusty plasmas, for an overview see e.g. [4, 5, 6, 7, 8]. Intense studies of trapped strongly correlated ions were performed in the last two decades of the previous century demonstrating, in particular the possibility of three-dimensional Coulomb crystals [9, 10, 11]. In parallel, a large number of theoretical and numerical investigations of Coulomb crystals was performed over the last 15 years, see e.g. [12, 13, 14, 15, 16, 17, 18] and references therein.

Meanwhile the experimental methods in many fields have improved essentially allowing to investigate in detail the structure of three-dimensional plasma crystals. Three-dimensional spherical dust crystals were recently observed at room temperature [19], and it was shown by computer simulations that their structure is very well explained by a statically screened Coulomb repulsion together with a constant parabolic confinement [20], in contrast to alternative theoretical models [21, 22].

These strongly correlated charged particle systems are a new and intesting kind of plasmas far outside the "normal" parameter range. Here many questions are still open. For completeness, we mention our recent theoretical investigations of the Coulomb crystallization conditions in a two-component plasma [23] and our analysis of macroscopic charged particle systems in traps, see Ref. [24] in this volume.

In this paper we will consider finite (mesoscopic) charged particle systems in a trap. In particular we will analyze the total energy. The trap is assumed to be realized by a parabolic potential and confines the particles thereby taking over the role of a neutralizing background which otherwise is needed to compensate the repulsive forces of the charged particles. We consider, thus, a true one component plasma (OCP) in a trap in contrast to the OCP (or jellium) model. Further, we discuss the transition to a macroscopic system.

2. Total Energy

The statistical expression for the total energy of a system of charge carriers is given by Eq. (1) and consists of three parts, e.g. [8]: the first is an ideal part (i.e. a contribution without correlations between the charged particles), E^0, first line of Eq. (1)). Second, a contribution which corresponds to the self–consistent field and [to be complemented, in a quantum system, by the corresponding exchange part], second line of (1), which is referred to as Hartree and Hartree–Fock terms E^H and E^{HF}, respectively. The third and most interesting contribution is the correlation energy, third line of (1), mediated by the Coulomb interaction between the charged particles, denoted by E^{corr}.

$$\begin{aligned} E_R &= \frac{3}{2}Nk_BT + \int d\mathbf{r}_1 n(\mathbf{r}_1) e\Phi_R(\mathbf{r}_1) \\ &+ \frac{1}{2}\int d\mathbf{r}_1 d\mathbf{r}_2 n(\mathbf{r}_1) n(\mathbf{r}_2) e^2 G(\mathbf{r}_1|\mathbf{r}_2) \\ &+ \frac{1}{2}\int d\mathbf{r}_1 d\mathbf{r}_2 n(\mathbf{r}_1) n(\mathbf{r}_2) g_{12}(\mathbf{r}_1,\mathbf{r}_2) e^2 G(\mathbf{r}_1|\mathbf{r}_2)\,, \end{aligned} \tag{1}$$

where $G(\mathbf{r}_1|\mathbf{r}_2)$ is the Green's function which may account for boundary conditions [8] which, in the following, will be replaced by $\frac{1}{|\mathbf{r}_1-\mathbf{r}_2|}$. Each of the terms of Eq. (1) depends on the trap potential which we will assume the to be given by

$$U = e\Phi_R(\mathbf{r}) = cr^2\,. \tag{2}$$

The inhomogeneity caused by the trap, in principle, affects all statistical quantities of the plasma, including the single particle distribution (density) $n(\mathbf{r})$ and the the two–particle distribution function F_{12} or two-particle correlation function g_{12}. In case of a weakly inhomogeneous system, these space dependencies can be simplified by a gradient expansion. To this end, one introduces center of mass and relative coordinates, $\mathbf{r}_1, \mathbf{r}_2 \to \mathbf{r}_1 - \mathbf{r}_2$, $\frac{1}{2}(\mathbf{R} = \mathbf{r}_1 + \mathbf{r}_2)$. Weak inhomogeneity then means that the relative and center of mass coordinates decouple, i.e. the pair correlation function g_{12} changes on much smaller scales in space than the single particle distribution $n(\mathbf{r})$ does, see our discussion in Ref. [24]. Then F_{12} is represented by

$$F_{12}(\mathbf{r}_1,\mathbf{r}_2) = n(\mathbf{r}_1)n(\mathbf{r}_2)[1 + g_{12}(\mathbf{r}_1 - \mathbf{r}_2); \mathbf{R}]\,,$$

where the correlation function g_{12} depends on the difference variables only, accept for a possible weak (parametric) dependence on $\mathbf{R}$. This is the local approximation. Otherwise one has to perform a gradient expansion and solve the equation for g_{12}, i.e. the second equation of the BBGKY hierarchy [24] more rigorously; see [8], p.131, for a discussion. We mention that the total energy of interacting quantum particles in an external potential was given in a quantum statistical formulation in several monographs, see, e.g., [25], [26]-[28].

The aim of this paper is to investigate some aspects of the space dependence of the thermodynamic quantities for the case of a finite (mesoscopic) system in a spherically symmetric parabolic trap. We will concentrate on the ground state, which is characterized by a shell structure. Here comparisons are possible with MD simulations and with experiments. Also, we consider different versions of analytical *onion shell models* of such mesoscopic clusters. Finally, we discuss the transition to a macroscopic system.

3. Shell models for the Ground State of Finite Systems

3.1. Ion sphere models of Hasse/Avilov and Tsuruta/Ichimaru

For the discussion of Coulomb clusters, Ichimaru and Tsuruta [13], Hasse and Avilov [12] and others introduced the *onion shell* model of Coulomb clusters of particles with charge

Ze. The energy of such clusters having shells is usually discussed on the basis of the Hartree approximation only which, in an infinite system, is divergent and has to be compensated by a neutralizing background. On the other hand, if there is a confining trap, there is no divergency, and no compensation is required.

The formula proposed by Tsuruta and Ichimaru reads [13] (energy per particle in units Ze^2/a)

$$\frac{E_{model}(N)}{N(Ze)^2/a} = 2^{1/3} \sum_{\nu=1}^{L} \frac{N_\nu}{N x_\nu} \left(\frac{N_\nu - \sqrt{N}_\nu}{2} + \frac{1}{2} x_\nu^3 + \sum_{\mu<\nu} N_\mu + \zeta \right) - \frac{9}{10} N^{2/3} \,, \tag{3}$$

where the dimensionless shell radii are $x_\nu = R_\nu/a$. The quantity $\zeta = 0; 1$ accounts for the possibility of zero or one particle being located exactly in the center, and the x_ν^2–term represents the potential energy of a compensating homogeneous background. The latter term originates from assuming a spherically symmetric background charge distribution which produces (inside the sphere) a parabolic potential.

On the other hand, the formula given by Hasse and Avilov is [12]

$$\epsilon_{\rm Coul} + \epsilon_{\rm conf} = \sum_{\nu=1}^{L} \left(\frac{N_\nu}{N R_\nu} \frac{N_\nu}{2} + \frac{1}{2N} N_\nu R_\nu^2 + \sum_{\mu<\nu} \frac{N_\nu N_\mu}{N R_\nu} \right) . \tag{4}$$

In Eqs. (3,4), the sum over μ represents the interaction of the particles in shell ν with those located on the shells *inside* the shell ν. This means, shell ν is assumed to be well separated from the other shells.

Shell models are based on formulae for charged spheres and spherical capacitors which we, therefore, briefly summarize, see also Ref. [33]. For example, a homogeneously charged sphere of radius a and total charge q, has the potential energy

$$E_{\rm sphere} = \frac{3}{5} \frac{q^2}{a} \,. \tag{5}$$

If the charge is homogeneously distributed over the surface of a sphere, we have (spherical capacitor)

$$E_{\rm surface} = \frac{1}{2} \frac{q^2}{a} \,. \tag{6}$$

Further, the electrostatic potential outside a charged sphere or surface at a distance r from its center is that of an equivalent point charge located in the center

$$\phi_{\rm point}(r) = \frac{q}{r} \,. \tag{7}$$

Next, if the total charge q of the sphere or of the spherical shell surface is made of N discrete elementary point charges, $q = Ne$, the expressions (5, 6) are modified to

$$E_{\rm sphere}(N) = \frac{3}{5} \frac{N(N-1)e^2}{a} \,. \tag{8}$$

and for the surface case (spherical capacitor)

$$E_{\rm surface}(N) = \frac{1}{2} \frac{N(N-1)e^2}{a} \,. \tag{9}$$

This is readily derived by counting the number of pair interactions. For example, Eq. (9) follows directly from Eq. (7): each of the N charges contributes an interaction energy $e \times \phi_{\rm point}(a)$

where $\phi_{\rm point}$ originates from the remaining $N-1$ charges, and the factor $1/2$ accounts for the double counting in the choice of pairs.

Shell models assume that all particles are located on concentric spherical layers of zero thickness and are thus directly related to the surface expressions (6,9) and (7). The exact discrete N particle system is thus mapped onto a system with homogeneous charge distribution. The only thing left to do is to count the number of pair interactions inside each shell and between shells which are given, respectively, by the first and third terms in the models (3) and (4). The intershell interaction depends on the charge inside a given radius, cf. Eq. (7), whereas the intrashell contributions should, according to Eq. (9), contain factors of the type $N_\nu(N_\nu-1)/2$ [the correction -1 is missing in the model (4)]. Comparison with the statistical energy expression (1) reveals that these intrashell and intershell terms correspond to the mean field (Hartree) contributions.

However, this simple counting argument neglects correlations in the intrashell distribution of the particles, i.e. the fact that the distribution of $N-1$ particles on a given shell in the exact system is not homogeneous, but disturbed by the $N-$th particle. Therefore, for a physically more accurate treatment of the interaction of charges inside the surface of a shell, the authors of Ref. [13] took into account that each of the N_ν particles on shell ν occupies a finite area of the size $A_{\nu,p}=4\pi R_\nu^2/N_\nu$ which cannot be occupied by other particles. This leads to a reduction of the intrashell interaction because each particle interacts with a charged surface of an area reduced by $A_{\nu,p}$ which gives rise to the square root term in the model(3). [This particular expression appears if the interaction energy of a sphere with area $A_{\nu,p}$ (i.e. with radius $R_\nu/\sqrt{N_\nu}$) with all particles on the shell is subtracted, which is more an "educated guess" than a derivation]. Comparison with Eq. (1) reveals that this square root term corresponds to correlations (beyond Hartree-Fock), i.e. to the last term in Eq. (1). It turns out that these correlation contributions which are missing in the model (4) are essential for an adequate shell model.

3.2. Improved shell model

In fact, the approximation for the correlations used in Eq. (3) is also only qualitatively correct. This is readily seen on the example of 2 particles (they occupy a single "shell" of radius a). Model (4) yields the Coulomb energy $\epsilon^H_{Coul}=N_\nu^2e^2/2a=2e^2/a$ with $N_\nu=2$. In contrast, the exact Coulomb energy is of course $\epsilon^{exact}_{Coul}=e^2/2a$ because in the ground state the two particles are located opposite to each other, each at a distance a from the trap center (total distance $2a$). The energy based on the correct pair counting, Eq. (9), is $\epsilon^{Eq.(9)}_{Coul}=e^2/a$, i.e. it is a factor 2 better than the model (4), but still a factor 2 wrong. This discrepancy arises from the model assumption of *homogeneous charge distribution* along the shell which is in this case, obviously, very far from the true location of the two particles. This difference is a clear effect of spatial correlations which become particularly obvious in this example. Interestingly, the model (3) performs much better giving $\epsilon^I_{Coul}=e^2/2a\times 2(2-\sqrt{2})$, which is wrong only by a factor 1.1716.

Now, we can turn the problem around: we can *force exact agreement* with a slight modification of model (3) by introducing an additional parameter ϵ in front of the square root, resulting in intrashell terms of the form $N_\nu(N_\nu-\epsilon\sqrt{N_\nu})/2$. Thus, our improved shell model becomes

$$\frac{E_{model}(N)}{N(Ze)^2/a}=2^{1/3}\sum_{\nu=1}^{L}\frac{N_\nu}{Nx_\nu}\left(\left[\frac{N_\nu-\epsilon\sqrt{N_\nu}}{2}+\sum_{\mu<\nu}N_\mu+\zeta\right]+\frac{1}{2}x_\nu^3\right)-\frac{9}{10}N^{2/3}\,, \qquad (10)$$

where, for simplicity, we assume that ϵ is the same for all shells.

For the present case of 2 particles, we obtain $\epsilon(2)=3/(2\sqrt{2})\approx 1.06066$. As we will see below, this slight modification of model (3) works not only for 2 particles but for arbitrary particle numbers. Of course, ϵ depends on N but very weakly. For example, for $N=3$, the exact ground state result is reproduced with the choice $\epsilon(3)=\sqrt{3}-2/3\approx 1.0654$, and for

$N = 4$, one finds $\epsilon(4) = 2 - (3/2)^{3/2}/2 \approx 1.08144$. As a final example, we give the exact value for $N = 6$: $\epsilon(6) = 11/2\sqrt{6} - 2/\sqrt{3} \approx 1.09067$. More values will be obtained numerically by comparison to the MD results, cf. Tab. 1. Interestingly, for large N the correlation parameter ϵ approaches a value of approximately 1.104 which allows to accurately reproduce the exact ground state energy. The reason for this surprisingly good behavior is that the functional form of the correlation term (the square root behavior) is an excellent approximation, although a satisfactory derivation is still missing.

4. Evaluation of the Shell Models

The practical value of the shell models is that they reduce many-body problem to a much less complex problem. Whereas the exact ground state requires the knowledge of the positions of all particles, in the shell models the number of free parameters is drastically reduced: one has to determine the number of shells, their populations N_ν and their radii R_ν. In addition, in the models (3) and (10) the parameter ζ has to be determined and, in the case of the improved model (10), also ϵ. This can be done for example with the help of a variational procedure. We now turn to the evaluation of the different models starting with the model (3).

4.1. Evaluation of the Shell Model (3)

We look for the lowest energy value of (3) by varying the occupation numbers $N_1 \cdots N_L$ and the radii $x_1 \cdots x_L$ under the condition $\sum_\nu N_\nu = N$. This means, we have, for a given number N, to find the number of shells L and their radii x_ν and occupation numbers N_ν.

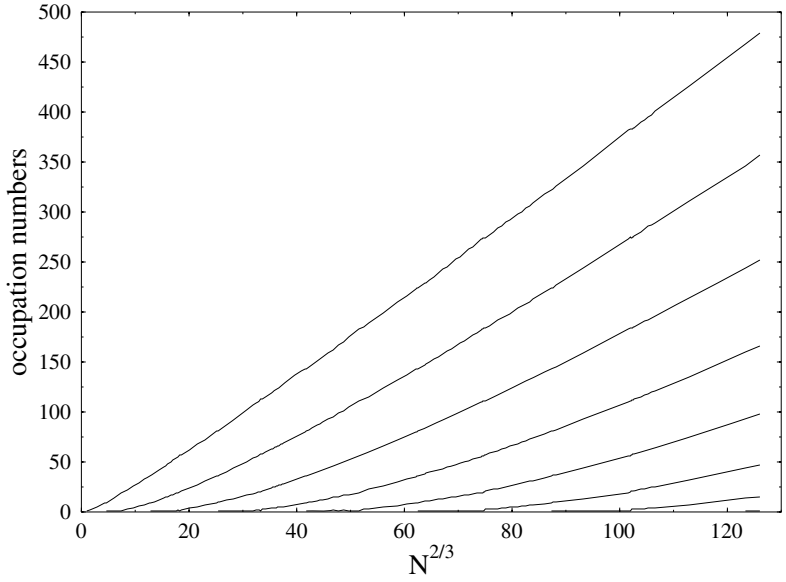

Figure 1. Shell occupation numbers from the Tsuruta & Ichimaru scheme Eq. (3) over $N^{2/3}$

We begin the procedure by first *assuming* the occupation numbers N_ν of each shell ν given such that $N = \sum_\nu^L N_\nu$. Then the radii of the shells x_ν follow from the condition $\partial E/\partial x_\nu = 0$ what gives the formula for the radii under the assumption that the occupation numbers are known. We have to determine $\partial E/\partial x_\nu$ from (3) and obtain

$$x_\nu = \left(\frac{N_\nu - N_\nu^{1/2}}{2} + \sum_{\mu<\nu} N_\mu + \zeta \right)^{1/3} \frac{1}{2^{1/3}} \,. \tag{11}$$

Now we have to perform a variation of the occupation numbers such that the minimum energy is found.

In principle, one has to vary any N_ν from 0 to N. In practice, it is sufficient to vary the N_ν around some *guess*, e.g., $N_\nu = N_\nu^{\rm guess} - 5 \cdots N_\nu^{\rm guess} + 5$. In the case of three shells, an independent variation is necessary for two shells only, so that we have to determine the energy, in our example, for 11×11 combinations and to select the lowest energy value, provided the range of variation around our guess includes the position of the minimum. For small particle numbers, the onsets of new shells are well known, see e.g. [17, 23] and the cited references: in a system with pure Coulomb interaction, the second shell starts at $N = 13$, the third from $N = 58$ (except for $N = 60$), the fourth shell starts at $N = 155$ and the fifth at $N = 311$ and so on. However, this procuedure works also if the number of shells is not known a priori. Then one has to vary both the occupation numbers *and* the number of shells in order to arrive at the well defined energy minimum.

The results of the evaluation are given in the following figures. First, we observe that the shell occupation numbers tend to a linear behavior as function of $N^{2/3}$, see Fig. 1, see also Ref. [23]. In Fig. 7, we show this again in a different scaling: for large N the normalized energy divided by $N^{2/3}$ tends to a constant. At the same time, the radius of the cluster tends to a $N^{1/3}$-dependence [23] which is also observed in the experiments with Coulomb balls [23] although there the interaction is statically screened (Yukawa). It turns out that this average scaling of the shell populations and radii (in units of the average distance) is insensitive to the pair interaction. On the other hand, the absolute values of the shell populations do depend on the interaction.

This scaling behavior means that the total energy, for large N, behaves like $N^{5/3}$, as can be seen directly from the model (3). It is interesting to note that this behavior is rather universal: it is also found for N harmonic oscillators at $T = 0$ [24] as well as for the energy of an ideal degenerate Fermi system. We will consider the behavior or a Fermi gas, including correlation effects later in the final section 5.

In the following Tab. 1, some results for the evaluation of Eq.(3) are given in the respective first of the three lines given for any N. For the second (and third) lines with $\epsilon > 1$ see next section. MD means the results from Molecular Dynamics calculations, [17], [30].

4.2. Evaluation of the improved Onion Shell Model (10)

We now consider the modified shell model (10) which includes an improved treatment of intrashell correlations by means of the additional parameter ϵ. We will compare the shell model results for different values of ϵ to MD simulations which will allow us to determine the optimal value of ϵ

We have to proceed in the same manner as before. For given occupation numbers, we determine the equations for the radii of the shells from the derivatives of (10), namely

$$x_\nu = \left(\frac{N_\nu - \epsilon N_\nu^{1/2}}{2} + \sum_{\mu<\nu} N_\mu + \zeta \right)^{1/3} \frac{1}{2^{1/3}} \,. \tag{12}$$

Another possible modification is the application of a Yukawa type potential

$$\frac{1}{x_\nu} \to \frac{\exp(-y x_\nu)}{x_\nu}$$

instead of the Coulomb potential. This potential is useful for complex systems where the screening exponent of the Yukawa potential models the influence of the surrounding medium

Table 1. Ground state energies, shell occupation numbers and radii for different N. First lines of the triples (quadruples): $\epsilon = 1$, model (3). Second (and third) lines: ϵ values and E_ϵ according to Eq. (10) such that $E_\epsilon \geq E_{MD}$. First two lines of the triples: Variation of both numbers of shells and respective occupation numbers. Lines labelled "MD" contain data from Refs. [17, 30]

N	ϵ	E/N	occupation	radii					
5	1.000	2.344764	5	0.8840					
5	1.077	2.246348	5	0.8653					
5	MD	2.245187	5	0.865					
10	1.000	4.288995	10	1.1957					
10	1.088	4.165116	10	1.1782					
10	MD	4.164990	10	1.178					
20	1.000	7.372128	19/1	1.6083					
20	1.095	7.249317	19/1	1.5948					
20	MD	7.247181	19/1	1.594					
30	1.000	9.969195	26/4	1.9332	0.7937				
30	1.098	9.840117	26/4	1.9220	0.7668				
30	MD	9.838964	26/4	1.919	0.796				
40	1.000	12.282618	33/7	2.1767	1.0286				
40	1.100	12.150509	34/6	2.1469	0.9384				
40	MD	12.150162	34/6	2.145	0.954				
50	1.000	14.410196	39/11	2.3921	1.2430				
50	1.100	14.277020	41/9	2.3506	1.1253				
50	MD	14.275728	41/9	2.349	1.137				
60	1.000	16.395254	45/14/1	2.5749	1.4525				
60	1.102	16.263771	46/13/1	2.5525	1.4021				
60	MD	16.263707	48/12/0	2.523	1.275				
160	1.000	32.436654	97/47/15/1	3.7630	2.6224	1.4860			
160	1.101	32.305332	101/46/12/1	3.7321	2.5269	1.3657			
160	MD	32.300404	102/45/12/1	3.7238	2.5161	1.3833			
190	1.000	36.494440	111/57/20/2	4.0128	2.8587	1.6964	0.5271		
190	1.100	36.361797	115/55/18/2	3.9858	2.7897	1.6303	0.4807		
190	MD	36.356674	115/56/18/1	3.98	2.78	1.58	0.004		
225	1.000	40.965789	126/67/27/5	4.2762	3.1313	1.9959	0.8840		
225	1.103	40.828812	132/67/24/2	4.2419	3.0181	1.7809	0.4791		
225	MD	40.827824	130/67/24/4	4.25	3.05	1.89	0.82		
300	1.000	49.834161	156/90/42/12	4.7604	3.6121	2.4596	1.2874		
300	1.104	49.695530	164/90/38/8	4.7246	3.5001	2.2765	1.0683		
300	MD	49.695467	160/91/40/9	4.73	3.53	2.34	1.15		
311	1.000	51.069141	159/92/44/14/2	4.8288	3.6987	2.5884	1.5275	0.5271	
311	1.105	50.931072	167/93/40/9/2	4.7940	3.5852	2.3958	1.3428	0.4781	
311	MD	50.929803	166/89/43/12/1	4.81	3.61	2.40	1.40	0.08	
503	1.000	70.736162	227/146/82/37/10/1	5.7588	4.6179	3.4825	2.3650	1.3024	
503	1.104	70.597836	240/148/79/31/5/0	5.7207	4.5002	3.28026	2.0577	0.8585	
503	1.105	70.596483	240/148/79/31/5/0	5.7207	4.5002	3.2802	2.0576	0.8582	
503	MD	70.596901	238/147/80/32/6	5.72	4.52	3.32	2.12	0.98	
561	1.000	76.148171	246/161/94/45/14/1	5.9914	4.8499	3.7102	2.5749	1.4525	
561	1.105	76.009222	259/163/90/39/9/1	5.9562	4.7433	3.5404	2.3528	1.2431	
561	MD	76.008582	257/161/88/42/12/1	5.957	4.760	3.680	2.501	1.402	0.09
565	1.000	76.514372	248/162/95/45/14/1	6.0052	4.8603	3.7160	2.5749	1.4525	
565	1.105	76.375380	260/165/91/39/9/1	5.9725	4.7578	3.5467	2.3528	1.2431	
565	MD	76.374771	258/162/89/43/12/1	5.973	4.780	3.740	2.510	1.404	0.12

Table 2. Continuation of Tab. 1

N	ϵ	E/N	occupation	radii					
570	1.000	76.970909	249/163/96/46/15/1	6.0258	4.8848	3.7456	2.6112	1.4860	
570	1.104	76.833220	262/166/92/40/9/1	5.9910	4.7760	3.5761	2.3665	1.2433	
570	MD	76.831249	258/166/90/43/12/1	5.997	4.810	3.760	2.260	1.400	0.03
585	1.000	78.332588	254/167/99/48/16/1	6.0823	4.9395	3.7974	2.6575	1.5182	
585	1.104	78.194768	267/170/95/42/10/1	6.0481	4.8331	3.6231	2.4222	1.2860	
585	MD	78.193046	264/170/93/45/12/1	6.0507	4.840	3.670	2.533	1.398	0.07
634	1.000	82.702137	270/180/109/55/19/1	6.2606	5.1127	3.9608	2.7976	1.6083	
634	1.104	82.563811	283/183/105/48/14/1	6.2283	5.0135	3.8011	2.6005	1.4369	
634	MD	82.562428	280/177/109/52/15/1	6.232	5.040	3.892	2.682	1.497	0.02
888	1.000	103.777149	342/241/157/91/43/13/1	7.0732	5.9332	4.7931	3.6559	2.5256	1.4175
888	1.104	103.638856	363/248/154/83/34/6/0	7.0338	5.8103	4.5879	3.3689	2.1465	0.9374
888	MD	103.637266	358/248/148/86/39/9	7.040	5.832	4.50	3.50	2.315	1.160
923	1.000	106.512044	353/249/163/96/46/15/1	7.1696	6.0258	4.8848	3.7456	2.6112	1.4860
923	1.104	106.373748	373/256/161/88/37/8/0	7.1329	5.9115	4.6913	3.4735	2.2618	1.0683
923	MD	106.371894	366/253/161/88/42/12/1	7.141	5.952	4.770	3.720	2.70	1.401
1024	1.000	114.217520	382/273/183/110/56/19/1	7.4387	6.2880	5.1345	3.9764	2.8075	1.6083
1024	1.104	114.079094	401/280/180/102/47/13/1	7.4060	6.1874	4.9704	3.7613	2.5641	1.4018
1024	MD	114.077248	392/275/183/107/51/15/1	7.415	6.230	5.180	3.990	2.674	1.499

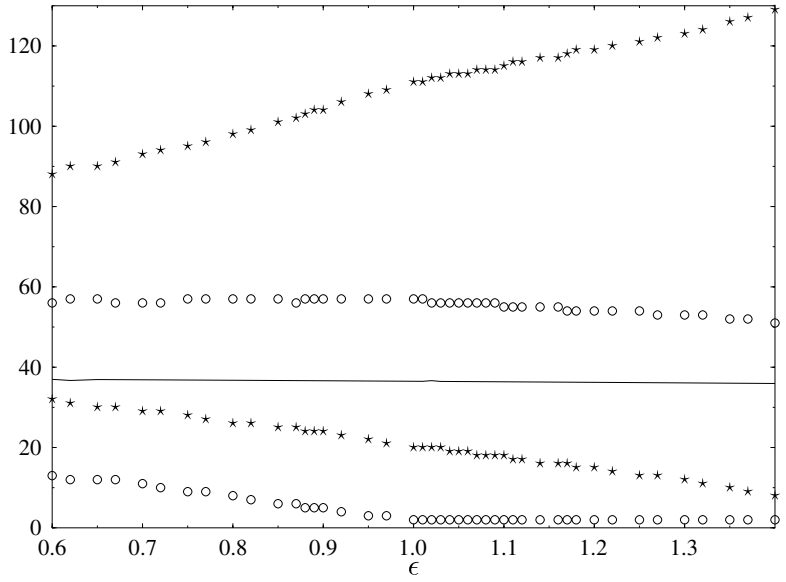

Figure 2. Numbers of particles on the shells and energy in *ryd* (full line) for $N = 190$ as a function of the correlation factor ϵ

on the two–particle interaction, e.g., in a dusty plasma [15] and for Coulomb balls [23] and will be discussed elsewhere. In general, i.e., for other than Coulomb potentials, the radii have to be determined numerically from the zeroes of the derivative of the total energy (10), i.e. of

$$R(x_\nu) = -\frac{1}{x_\nu^2}\left[\frac{N_\nu - \epsilon\sqrt{N}_\nu}{2} + \sum_{\mu<\nu} N_\mu + \zeta\right] + x_\nu = 0\,. \tag{13}$$

Table 3. Energies, shell occupation numbers and radii for $N = 160$ for different ϵ values. Comparison with Ref. [17] (denoted "LKB05")

ϵ	E/N	occupation	radii		
1.000	32.436654	97/47/15/1	3.7630	2.6224	1.4860
1.030	32.397552	98/47/14/1	3.7551	2.5954	1.4480
1.060	32.358222	100/46/13/1	3.7408	2.5562	1.4085
1.080	32.331799	100/46/13/1	3.7396	2.5544	1.4055
1.100	32.305332	101/46/12/1	3.7321	2.5269	1.3657
1.104	32.300008	101/46/12/1	3.7319	2.5265	1.3651
1.105	32.298677	101/46/12/1	3.7318	2.5264	1.3649
1.110	32.292021	101/46/12/1	3.7315	2.5260	1.3641
1.120	32.278707	101/46/12/1	3.7309	2.5251	1.3626
LKB05	**32.300404**	102/45/12/1	3.7238	2.5161	1.3833

The procedure is performed according to an iteration of

$$x_\nu^{(1)} = x_\nu^{(0)} - \frac{R_\nu(x_\nu^{(0)})}{R'_\nu(x_\nu^{(0)})}\,. \tag{14}$$

Here, $R'(x_\nu)$ is the partial derivative of $R(x_\nu)$ with respect to x_ν. In Eq. (10), the x_ν- dependence was not changed, so that we could immediately use Eq. (11).

In the following figures and tables, we give some numerical results. In Figs. 2 and 3, we see for the example of $N = 190$ that the occupation numbers and the shell radii vary considerably with ϵ, while the energy is changed only slightly. A numerical example is given in Tab. 2 for $N = 160$. In Tab.2, also the corresponding MD result is indicated. From Tab. 3 we see, in

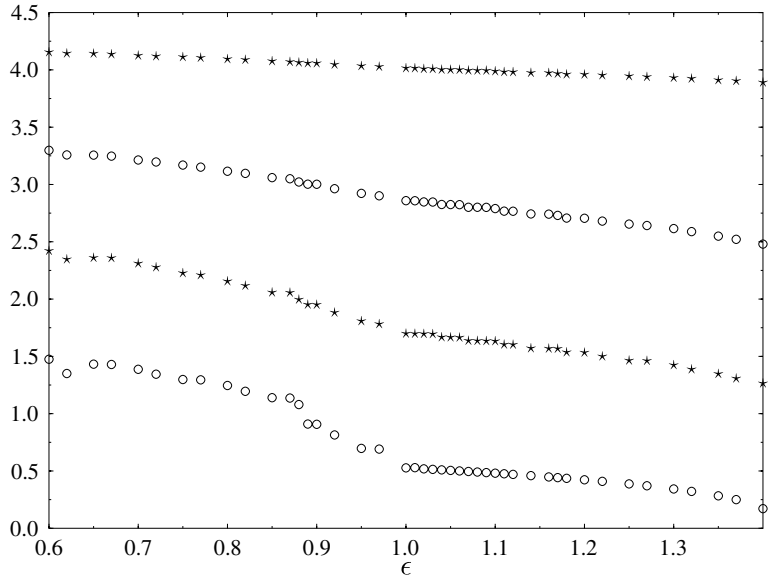

Figure 3. Shell radii in units of a_B for $N = 190$ as a function of the correlation factor ϵ

particular, that we get agreement with the MD data for ϵ–values around 1.1. On the other hand,

the energy keeps decreasing with ϵ without bound which is unphysical. Therefore, values of ϵ leading to ground state energies lower than the (exact) MD results are unphysical and will be excluded.

We follow two strategies:

1.) For N given, the minimum energy is determined from (10) by variation of the occupation numbers and thus of the radii for epsilon as a given parameter. The results of this scheme are presented in Tab. 2 and in Figs. 2 and 3. Then the parameter ϵ may be varied such that the MD energies are met. Some results are collected in Tab. 1; here the respective results of the second lines for any N were determined such that $E_\epsilon \geq E_{MD}$, where the MD results are given in the respective third lines.

The scheme described so far exhibits discrepancies between occupation numbers and radii. Therefore we also consider a second approach:

2.) We take the occupation numbers from MD, determine the energy according to Eq.(10) and find such ϵ values which give energies as close as possible to those from MD (see the respective third lines in table 1).

In Tab. 4 we see an excellent agreement between energies, occupation numbers and radii for $\epsilon = 1.104$ for several larger clusters. We give some comparison to the numerical results given in [17] and [30].

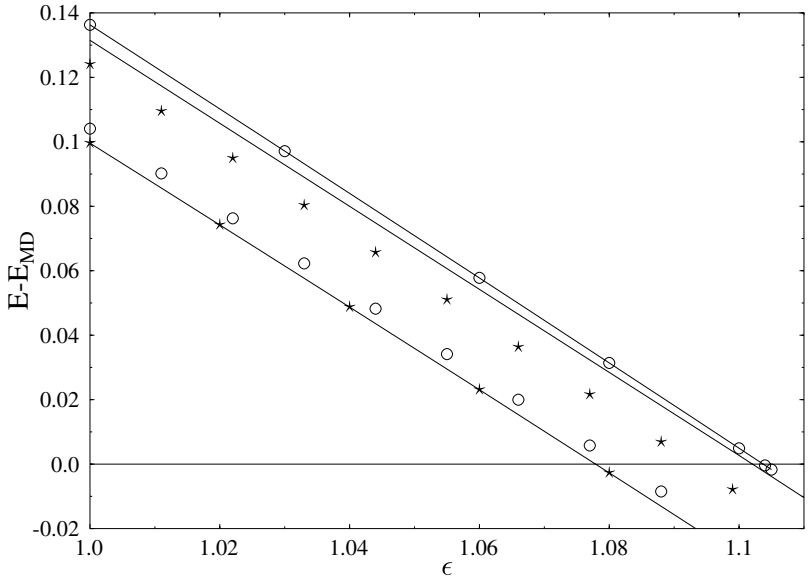

Figure 4. $E_\epsilon - E_{MD}$ over ϵ for various N. From below: N=5 (line with asterisks), N=4 (circles), 10 (asterisks), 60 (full line), N=160 (line with circles)

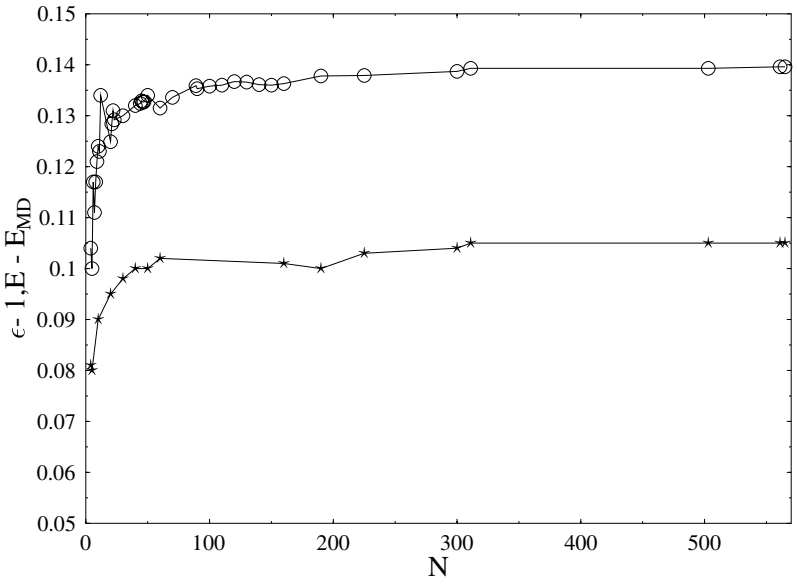

Figure 5. Deviation of Tsuruta/Ichimaru shell model energy from MD data (circles) and optimal value of $\epsilon - 1$ (asterisks) vs. N

Table 4. Energies, occupation numbers and radii for different N and for fitted ϵ values (to MD energies) and given occupation numbers taken from MD. Application of Eq.(10) for given N_ν (second lines). Comparison with MD results from Refs. [17] and [30] (first lines)

N	ϵ	E/N	occupation	radii				
225	MD	40.827824	130/67/24/4	4.25	3.05	1.89	0.82	
225	1.104	40.828006	like in MD	4.2516	3.0542	1.8803	0.7651	
300	MD	49.695467	160/91/40/9	4.73	3.53	2.34	1.15	
300	1.104	49.695782	like in MD	4.7401	3.5467	2.3364	1.1245	
503	MD	70.596901	238/147/80/32/6	5.72	4.52	3.32	2.12	0.98
503	1.104	70.597914	like in MD	5.7260	4.5209	3.3181	2.1133	0.9374

5. Discussion. Transition to a macroscopic plasma

5.1. Quality of the shell models

We first briefly discuss the quality of the shell models compared to the simulation results. The model (4) has the worst behavior which is due to the complecte neglect of intrashell correlation effects. Inclusion of these effects by the model of Tsuruta and Ichimaru, Eq. (3) significantly improves the quality. Comparison with the MD data, cf. Tab. 1, shows that the ground state energy is quite accurate: the relative error decreases from about 5% for $N = 5$ to about 0.3% for $N = 160$. Although this seems to be satisfactory, one has to keep in mind that these systems possess many metastable states which are energetically close to the ground state, see e.g. Ref. [17]. In fact, the deviations in energy of the model are sufficient to systematically miss the correct ground states starting approximately at $N = 40$. Also, the shell radii are systematically too large, indicating an overestimate of the Coulomb repulsion.

On the other hand, the improved shell model (10) shows in fact a much better behavior. Even for larger clusters, the shell radii and populations are much closer to the simulation results than in the model (3). This indicates that the increased correlation induced reduction of the

interparticle repulsion achieved with the parameter ϵ is physically relevant. The results show that best agreement with the simulations is reached for values of the correlation parameter ϵ close to 1. With increasing N, the optimal values approaches 1.104. We, therefore, expect that this value should have relevance also for a macroscopic plasma which we discuss below. On the other hand, from a practical stand point we may use the shell model (10) with the fixed parameter $\epsilon = 1.104$ to predict the ground state configuration of large clusters in the range from several thousands to hundred thousands where exact simulations are extremely costly, e.g. [14]. These data are also expected to be valuable for comparison with experimental results in dusty plasmas and trapped ion systems, although for the first case one still needs to extend the model to Yukawa systems.

5.2. Shell models and relation to macroscopic plasmas

We now compare the shell model results to available analytical formulas for a macroscopic homogeneous one-component Fermi system, i.e. in the absence of any confinement field (but with a compensating homogeneous background). Here, results for a classical OCP and for a degenerate quantum Fermi system are available which we briefly review. In particular, we consider weak coupling results (Debye approximation) for finite temperatures of $k_BT/ryd = 1$ and $k_BT/ryd = 0.01$, and also the zero temperature results due to Gell-Mann and Brueckner and Carr and Maradudin, respectively. At very high densities, i.e. at high degeneracy, the dependence on the temperature vanishes.

First, in the weakly coupled non-degenerate case, i.e., at low densities and high temperatures, the internal energy is approximated by the Debye law with $\kappa^2 = \frac{4\pi n e^2}{k_BT}$,

$$\frac{E}{N} - \frac{3}{2}k_BT = -k_BT\frac{\kappa^3}{12\pi n} = -\frac{2}{3}\left(\frac{8\pi n}{k_BT}\right)^{1/2} = -\frac{2}{3}\kappa\,,$$

where the second and third r.h.s. expressions are given in Heaviside–units ($2m_e = e^2/2 = \hbar = 1$):

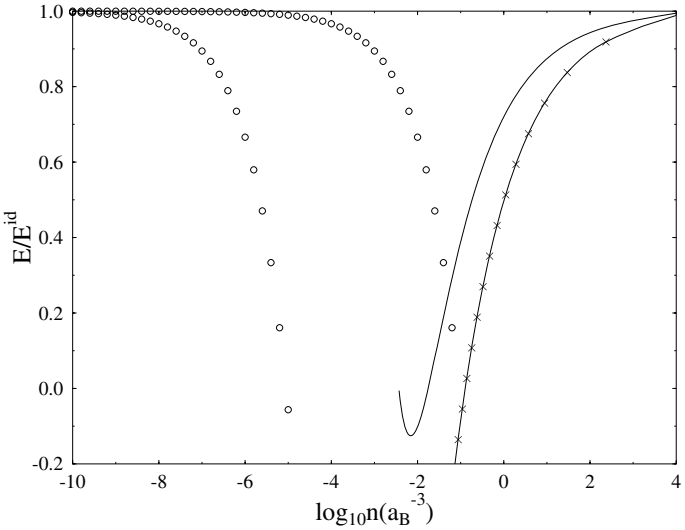

Figure 6. Energy in the Debye approximation (circles), left curve: $k_BT = 0.01ryd$, right curve: $k_BT = 1ryd$, in the Gell-Mann–Brueckner/Carr–Maradudin approximation (15) – full line, and in the Wigner approximation (16) – crosses.

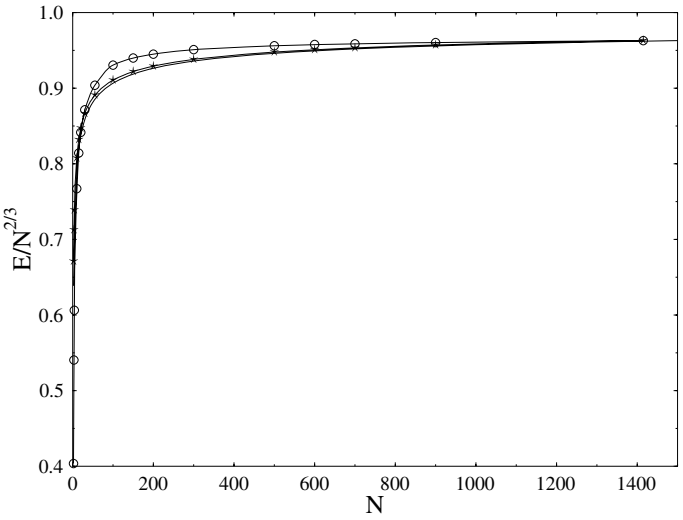

Figure 7. Normalized ground state energy vs. particle number according to the Tsurutra & Ichimaru scheme Eq. (3)(circles) and the degenerate OCP–model in two approximations according to (15): Asterisks- first three r.h.s terms, full line- full expression. Enlarged views are given in the subsequent figures

Secondly, the highly degenerate expression for the energy can be approximated by the following expressions, according to [35], [36] (for an overview see, e.g. [26], [28])

$$\frac{E}{N} = \frac{2.21}{r_s^2} - \frac{0.916}{r_s} + 0.0622 \ln r_s - 0.096 + 0.018 r_s \ln r_s \,, \tag{15}$$

where r_s is the Brueckner parameter (the quantum Coulomb coupling parameter) which is the ratio of the mean interparticle distance d and the Bohr radius a_B, $r_s = \frac{d}{a_B}$, and we use the hydrogen Bohr radius $a_B = 0.529 \times 10^{-8} cm$ below and $d = (\frac{3}{4\pi n})^{1/3}$.

Finally, the Wigner lattice result for an OCP at zero temperature is characterized by the energy

$$\frac{E_{Wigner} - E_{id}}{N} = -\frac{1.792}{r_s} \,. \tag{16}$$

The shell model results presented in Figs. 7 and 8 shows a similar shape as the formula (15). This fact is underlined by the explicit comparison with the Wigner result (16), as well as with the Hartree Fock energy

$$\frac{U_{HF}}{N} = -\frac{0.916}{r_s}. \tag{17}$$

The corresponding classical $T = 0$ result was derived by DeWitt, Slattery & Doolen [37], [38]; see also [39] and is given by

$$E_{cc} = -k_B T N_{ion} \times 0.89752 \Gamma \,. \tag{18}$$

Here the only relevant parameter is the nonideality parameter (classical Coulomb coupling parameter) given by $\Gamma = \frac{(Ze)^2}{k_B T} \left(\frac{4\pi N_e}{3ZV}\right)^{1/3}$. For large Γ–values, we have to take the Wigner result. Not that all three expressions, Eqs. (16), (17), and (18), which are corrections to the ideal energy (which scales like $N^{1/3}$), behave like $N^{1/3}$. The next order would be the logarithm, see e.g. expression (15).

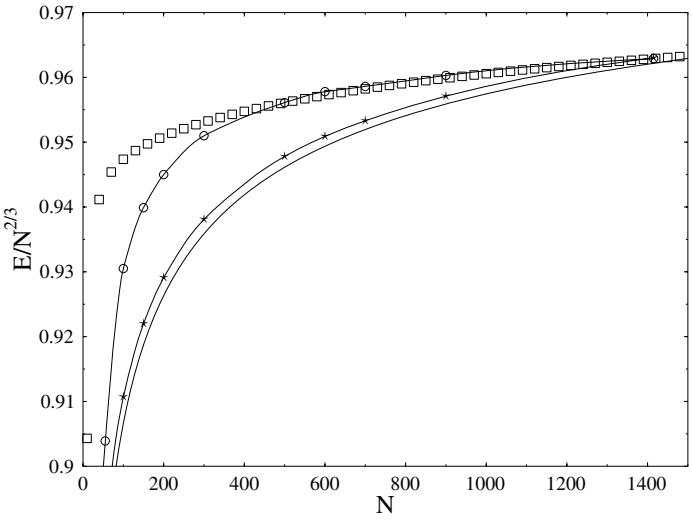

Figure 8. Same as Fig. 7, zooming into the energy scale. Approximations according to (15), asterisks- first three r.h.s terms, full line- full expression. In addition- squares according to the fit formula (19)

We now try to fit the results of the shell model to the known analytical schemes using the above asymptotics for large N. We, therefor, write the energy at $T = 0$ in the following form

$$\frac{E}{N} = AN^{2/3} - BN^{1/3} - C \ln N \,. \tag{19}$$

A first fit to the shell results for $N = 500$ and $N = 1415$ leads to the coefficients

$$B/A = 0.7381 \quad , \quad C/A = -0.4977 \,.$$

The results according to the (19) are indicated by squares in Fig. 8. If we assume the coefficient A to be that of the degenerate electron gas, as in Eq. (15), the result for B/A corresponds to $B = 1.6312$ close to the Wigner result of $B_W = 1.792$. As is obvious from Fig. 8, the agreement is very good for $N \geq 400$, whereas for smaller N the shell model (and exact) behavior is different. This trend is not surpising since the analytical asymptotics, and thus the fit ((19)) are valid only for large N.

A further improved ansatz would be

$$E/N = AN^{2/3} - BN^{1/3} - C \ln N - D + FN^{-1/3} \ln N + GN^{-1/3} + \cdots \,.$$

However, here we restrict ourselves to the first four terms,

$$\frac{E}{N} = AN^{2/3} - BN^{1/3} - C \ln N - D \,. \tag{20}$$

A fit to the results of the shell model (3) using the three points $N = 500, 900, 1415$ leads to

$$B/A = 1.0242 \ , \ C/A = -1.4026 \ , \ D/A = 3.3524 \,,$$

and the insertion into (20) leads to the data marked by diamonds in Fig. 9.
An alternative choice of the three points $N = 4, 100, 1415$ might be expected to reproduce the small N behavior and yields

$$B/A = 0.6786 \ , \ C/A = -0.4869 \ , \ D/A = 0.5898 \,.$$

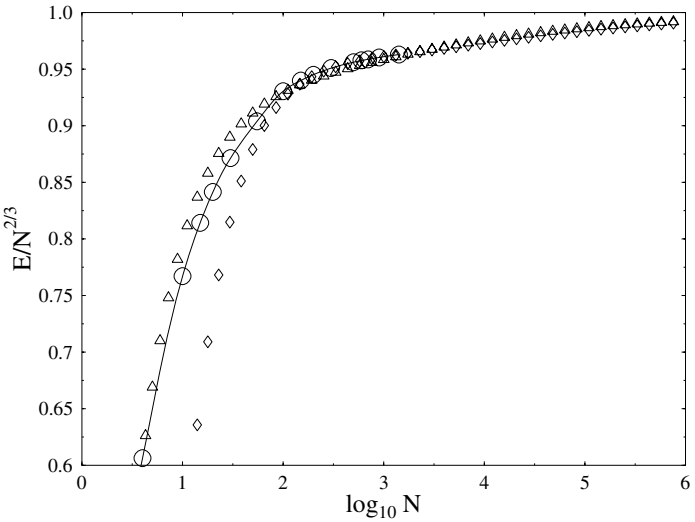

Figure 9. Tsuruta & Ichimaru scheme- circles. Diamonds and triangles- fit according to (20)

This approximation is shown by the triangles in Fig 9. For the same reason as noted above, this kind of fit applied to higher N–values is more reasonable. Then, there is a discrepancy in Figs. 8,9 for small N (only).

Finally, we perform a fit of the type (20) to the MD data for clusters with N up to 1024. The result is displayed in Fig. 10. Triangles correspond to a fit to $N = 5, 160, 1024$, (giving $B/A = 0.6586, C/A = -0.4612, D/A = 0.6219$) whereas the diamonds represent the fit to $N = 503, 888, 1024$, ($B/A = 1.077, C/A = -1.599, D/A = 4.289$)

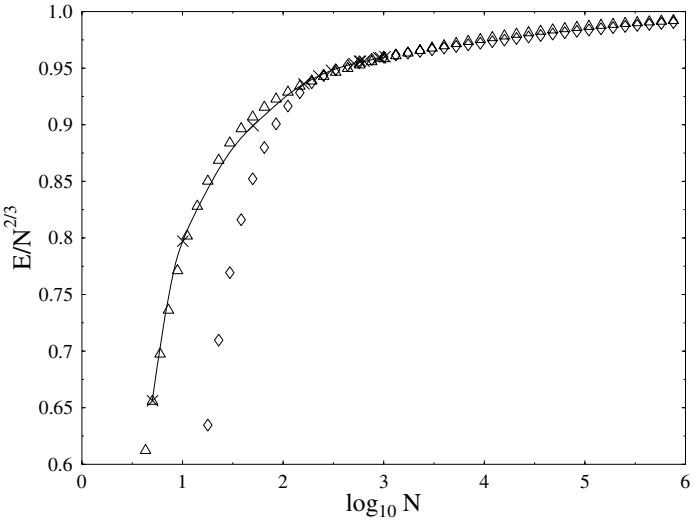

Figure 10. MD data- crosses. Diamonds and triangles- fit according to (20): triangles- fit to $N = 5, 160, 1024$; diamonds- fit to $N = 503, 888, 1024$

Finally, we note that there are no reliable results yet in the thermodynamic limit in the intermediate density and temperature range. Here one has to rely on first principle computer simulations, such as quantum Monte Carlo results, see, e.g., [40]-[44].

Acknowledgments
We thank V. Golubnychiy for providing us with MD data for large clusters. This work is supported by the Deutsche Forschungsgemeinschaft via SFB-TR24. One of us (WDK) wants to thank Ronald Redmer (Institute of Physics, Rostock University) for hospitality.

References

[1] Ashoori R C 1996, *Nature* (London) 379, 413
[2] Filinov A , Bonitz M, and Lozovik Yu E 2001, *Phys. Rev. Lett.* **86** 3851
[3] Major F, Gheorge V and Werth G 2005 *Charged Particle Traps. Physics and Techniques of Charged Particle Field Confinement* (Heidelberg: Springer)
[4] Thomas H and Morfill G E 1996 *Nature* (London) **379** 806
[5] Hayashi Y and Tachibana K 1994 *Jpn J Appl Phys* **33** L804
[6] Chu J H and I L 1994 *Physica* **205A** 183
[7] Melzer A, Homann A, and Piel A 1996 *Phys Rev E* **53** 2757
[8] Dubin D H E and O'Neil T M 1999 *Rev. Mod. Phys.* **71** 87
[9] Wineland D J, Bergquist J C, Itano W M, Bollinger J J, and Manney C H 1987 *PRL* **59** 2935
[10] Dietrich F, Peik E, Chen J E, Quint W, and Walther H 1987 *PRL* **59** 2931
[11] Itano W M, Bollinger J J, Tan J N, Jelenković B, and Wineland D J 1998 *Science* **279** 686
[12] Hasse R W and Avilov V V 1991 *Phys Rev A* **44** 4506
[13] Tsuruta K and Ichimaru S 1993 *Phys Rev A* **48** 1339
[14] Schiffer J P 2002 *Phys. Rev. Lett.* **88** 205003
[15] Totsuji C, Liman M S, Tsuruta K and Totsuji H 2003 *Phys. Rev. E* **68** 017401
[16] Totsuji H, Liman M S, Totsuji C and Tsuruta K 2004 *Phys. Rev. E* **70** 016405
[17] Ludwig P, Kosse S and Bonitz M 2005 *Phys Rev E* **71** 046403
[18] Arp 0, Block D, Bonitz M, Fehske H, Golubnychiy V, Kosse S, Ludwig P, Melzer A, and Piel A 2005 *Journal of Physics: Conference Series* **11**, 234
[19] Arp O, Block D, Piel A, and Melzer A 2004 *Phys. Rev. Lett.* **93** 165004
[20] Bonitz M, Block D, Arp O, Golubnichiy V, Baumgartner H, Ludwig P, Piel A, and Filinov A 2006, *Phys. Rev. Lett.* **96** 075001
[21] Totsuji H, Totsuji C, Ogawa T and Tsuruta K 2005 *Phys. Rev. E* **71** 045401(R)
[22] Chen Z Y, Yu M Y, and Luo H Q 2005, *Physica Scripta* **71** 638
[23] Bonitz M, Filinov V S, Fortov V E, Levashov P R, and Fehske H 2005 *PRL* **95** 235006
[24] Kraeft W D and Bonitz M 2006 *J Phys*, this volume
[25] Kadanoff L P and Baym G 1962 *Quantum Statistical Mechanics* (Redwood City, California: Addison-Wesley)
[26] Ebeling W, Kraeft W D and Kremp D 1976 [1979] *Theory of Bound States and Ionization Equilibrium in Plasmas and Solids* (Berlin [Moscow]: Akademie-Verlag [Mir])
[27] Kraeft W D, Kremp D, Ebeling W and Röpke G 1986 *Quantum Statistics of Charged Particle Systems* (Berlin[New York]: Akademie–Verlag[Plenum])
[28] Kremp D, Schlanges M and Kraeft W D 2005 *Quantum Statistics of Nonideal Plasmas* (Berlin/Heidelberg: Springer)
[29] Thomas H, Morfill G E, Demmel V, Goree J, Feuerbacher B, and Möhlmann D 1994 *PRL* **73** 652
[30] Golubnychiy V *unpublished*
[31] Ichimaru S 1982 *Rev. Mod. Phys.* **54** 1017
[32] Totsuji H, Kishemoto T, Totsuji C and Tsuruta K 2002 *Phys. Rev. Lett.* **88** 125002
[33] Feynman R P, Leighton R B and Sands M 1964 *The Feynman Lectures on Physics, Vol 2 & Exercises* (Reading Mass: Addison-Wesley)
[34] Tanatar B and Ceperley D M 1989 *Phys Rev B* **39** 5005
[35] Gell-Mann M and Brueckner K 1957 *Phys Rev* **106** 364
[36] Carr W J and Maradudin A A 1964 *Phys Rev* **133** 371
[37] DeWitt H E and Hubbard W B 1976 *ApJ* **205** 295
[38] Slattery W L and Doolen G D 1980 *Phys Rev A* **21** 2087
[39] Luo G Q 1997 *The Astrophysical Journal* **491** 366
[40] Militzer B and Ceperley D M 2001 *Phys Rev* **E63** 066404
[41] Vorberger J, Schlanges M and Kraeft W D 2004 *Phys Rev* **E69** 046407
[42] Knaup M, Reinhard P G and Toepffer C 2001 *Contrib Plasma Phys* **41** 159
[43] ACTEX–OPAL 2000 *http://www.pat.llnl.gov/Research/OPAL/Download*
[44] Filinov V S, Bonitz M, Ebeling W and Fortov V 2001 *Plasma Phys Controlled Fusion* **43** 743